Dalton Transactions

ROYAL SOCIETY OF CHEMISTRY

PAPER

View Article Online
View Journal | View Issue

Check for updates

Cite this: *Dalton Trans.*, 2023, **52**, 9017

Catalytic oxidation properties of an acid-resistant cross-bridged cyclen Fe(II) complex. Influence of the rigid donor backbone and protonation on the reactivity†

Jean-Noël Rebilly,* Christian Herrero, Katell Sénéchal-David, Régis Guillot and Frédéric Banse *

Received 7th February 2023,
Accepted 26th May 2023

DOI: 10.1039/d3dt00393k

rsc.li/dalton

The catalytic properties of an iron complex bearing a pentadentate cross-bridged ligand backbone are reported. With H_2O_2 as an oxidant, it displays moderate conversions in epoxidation and alkane hydroxylation and satisfactory ones in aromatic hydroxylation. Upon addition of an acid to the reaction medium, a significant enhancement in aromatic and alkene oxidation is observed. Spectroscopic analyses showed that accumulation of the expected $Fe^{III}(OOH)$ intermediate is limited under these conditions, unless an acid is added to the mixture. This is ascribed to the inertness induced by the cross-bridged ligand backbone, which is partly reduced under acidic conditions.

Introduction

Oxidation metalloenzymes are able to achieve oxidation catalysis under very mild conditions with high turnovers using O_2 as an oxidant.[1] To do so, they carry out the 2 electron reduction of dioxygen to generate a reactive species. In the best known systems, cytochromes P450, this leads to the generation of a (P)$Fe^{III}OOH$ intermediate, which is the precursor for the active species, compound I, a $(P^{\bullet+})Fe^{IV}$=O species (formally an Fe^{V}=O species).[2–4] Its formation results from the heterolytic cleavage of the peroxo bond of (P)$Fe^{III}OOH$. To achieve this, the push–pull effect is evoked to rationalize this favored pathway: a strongly donating 1st coordination sphere ("push") is associated with hydrogen bonding and cationic residues in the 2nd sphere that "pull" the electronic density at the distal oxygen atom.[3]

Non-heme iron models have been developed and allow accessing $Fe^{III}OOH$ intermediates starting from Fe^{II} and H_2O_2. Most of the time, with pentadentate aza ligands, $(N_5)Fe^{III}OOH$ follows a homolytic cleavage pathway, leading to an $\{Fe^{IV}$=O; $OH^{\bullet}\}$ pair.[5–10] With tetradentate aza ligands, $(N_4)Fe^{III}OOH$ is proposed to follow heterolytic cleavage, leading to an $(N_4)Fe^{V}$(=O)(OH) species, thanks to the presence of two *cis* exchangeable sites.[11–15] In the case of (TMC)Fe^{III}(OOH) (TMC = tetramethylcyclam), the two exchangeable sites are trans and the cleavage was proposed to be homolytic.[16] But upon addition of an acid, it could switch to heterolytic.[17] This trend was reported for other systems[18–20] and rationalized by protonation of the distal oxygen of the $Fe^{III}OOH$ adduct, which also induced an impact on the reactivity and selectivity towards substrates.

We recently showed that increasing the donating ability of a non-heme aminopyridine ligand by replacement of pyridines by phenolates had a drastic impact on the O_2 activation ability of the complex, thanks to an increased "push" effect.[21] Association of this push ability to an external acid activation of Fe^{III}(OOH) (pull effect) could strongly favor the heterolytic O–O bond cleavage and enhance the reactivity.

For this purpose, we report herein a complex derived from a cross-bridged cyclen ligand capable of increasing the push character thanks to a strong σ-donor character with respect to aminopyridine ligands and resistance to the acidic conditions required to achieve the pull effect. The reactivity towards various substrates in the presence of H_2O_2 was evaluated and shows that addition of an acid significantly enhances the conversions. Spectroscopic studies were also carried out and showed the formation of an $(N_5)Fe^{III}$(OOH) species in the absence of an acid, and an $(N_4)Fe^{III}$(OOH) species in the presence of an acid, with a dangling pyridinium.

Institut de Chimie Moléculaire et des Matériaux d'Orsay (ICMMO), 91405 Orsay cedex, France. E-mail: jean-noël.rebilly@universite-paris-saclay.fr, frederic.banse@universite-paris-saclay.fr

†Electronic supplementary information (ESI) available. CCDC 2184867 and 2184868. For ESI and crystallographic data in CIF or other electronic format see DOI: https://doi.org/10.1039/d3dt00393k

Results

Ligand and complex synthesis

The ligand cyclenCB–CH_2py (Chart 1) was synthesized according to a literature procedure.[22] The synthetic scheme follows a

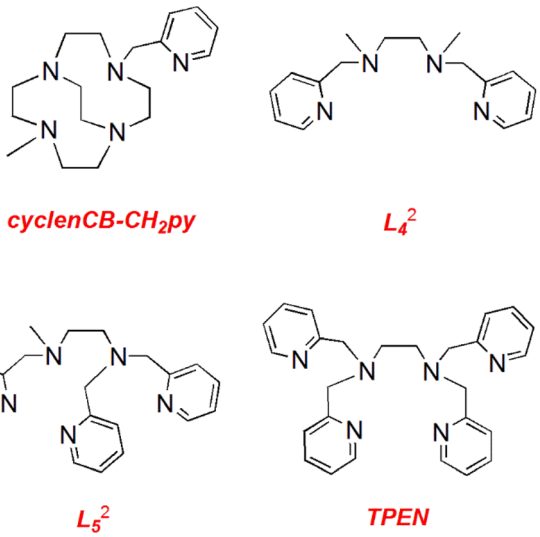

Chart 1 Structures of the ligands mentioned in this article.

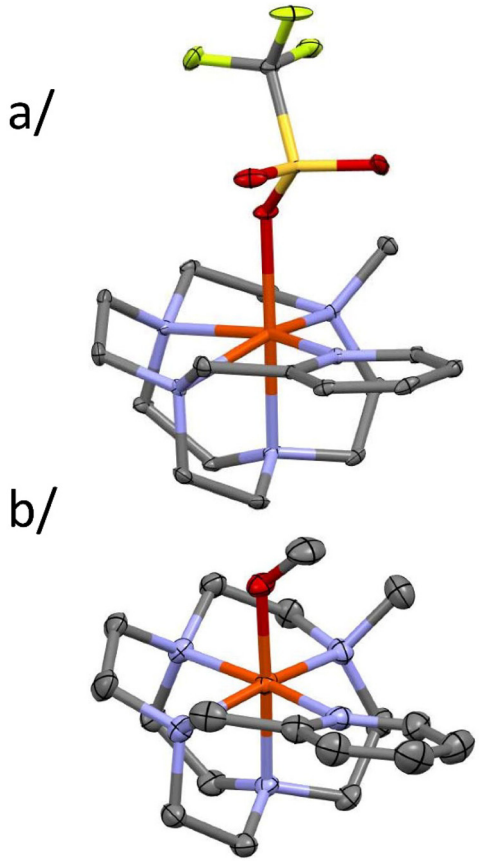

Fig. 1 An ORTEP drawing of the cation **[(cyclenCB–CH$_2$py)Fe^{II}(OTf)]$^+$** of **[(cyclenCB–CH$_2$py)Fe^{II}(OTf)](OTf)** (top) and of the cation **[(cyclenCB–CH$_2$py)Fe^{III}(OMe)]$^{2+}$** of **[(cyclenCB–CH$_2$py)Fe^{III}(OMe)](OTf)$_2$** (bottom). Thermal ellipsoids are shown at the 30% level. Fe is in orange-red, C is in grey, N is in blue, O is in dark red, S is in yellow, and F is in light green.

sequence of reactions starting with the formation of a cyclen/glyoxal bisaminal,[23,24] its sequential alkylation by two different groups,[25–27] and the reduction of the resulting dication to yield a cross-bridged bis-functionalized macrocycle.[25] The complex **[(cyclenCB–CH$_2$py)Fe^{II}(OTf)](OTf)** was synthesized as a tan powder in 75% yield by the addition of the ligand onto Fe^{II}(OTf)$_2$ in MeOH under Ar followed by precipitation with Et$_2$O. It was characterized by ESI-MS, UV-vis and NMR spectroscopy and cyclic voltammetry (Fig. S1–S7†). Single crystals suitable for X-ray diffraction were obtained by diffusion of diethyl ether into a methanolic solution of the complex and the structure is depicted in Fig. 1.

The iron center sits in a distorted octahedral environment resulting from the binding of the ligand in a pentadentate fashion, with the 6th position being occupied by a triflate anion. Cyclen and cross-bridged cyclen macrocycles are too constrained to be able to coordinate the metal in its 4 equatorial positions, and the pyridine and the triflate anion are thus bound *cis* to each other. The Fe–N bonds of the macrocycle sit within 2.15–2.22 Å, Fe–N$_{py}$ = 2.13 Å and Fe–O = 2.11 Å. These values are in the range observed for high spin complexes, in line with the binding of the triflate anion.[28] They also match the Fe–N bonds reported in other cross-bridged (cyclen)Fe complexes.[22,29–31]

The ^{1}H NMR spectrum in MeCN, observed in the [0, 9] ppm window, corresponds to a diamagnetic, and thus, low spin species indicating that the triflate ligand is likely substituted by MeCN in solution (Fig. S1–S3†). ESI-MS confirms the binding of cyclenCB–CH$_2$py and the weakness of the Fe–triflate bond (Fig. S4†). The cyclic voltammogram displays a reversible wave at $E_{1/2}$ = 0.71 V (ΔE = 100 mV) *vs.* SCE, ascribed to an Fe^{III}/Fe^{II} couple and a less reversible one at $E_{1/2}$ = −1.84 V (ΔE = 130 mV) *vs.* SCE, ascribed to an Fe^{II}/Fe^{I} couple (Fig. S6†). By comparison, the value reported for **[(cyclenCB–CH$_2$py)Fe^{II}Cl](PF$_6$)** was −0.285 V *vs.* Fc$^+$/Fc (approximately 0.095 mV *vs.* SCE) in DMF, but the couple was poorly reversible under these conditions. We thus added chloride (1 equiv. of NBu$_4$Cl) to **[(cyclenCB–CH$_2$py)Fe^{II}(OTf)](OTf)** in MeCN (Fig. S7†). If triflate was bound to iron in MeCN solution, it should be readily displaced by the more donating chloride, but the charge of the complex should remain +1 and the potential should be poorly affected. The main couple after the addition of 1 equiv. of chloride is $E_{1/2}$ = 0.4 V (ΔE = 100 mV), in line with a decrease of the global charge by coordination of an extra anion. Addition of a 2nd equiv. of chloride is characterized by a decrease in the intensity of these waves in favor of the growth of another couple at $E_{1/2}$ = 0.13 V (ΔE = 90 mV), consistent with the binding of a 2nd anion, and the detection of free chloride at $E_{1/2}$ = 1.1 V. These evolutions allow us to ascribe the initial couple at $E_{1/2}$ = 0.71 V (ΔE = 100 mV) to a **[(cyclenCB–CH$_2$py)Fe^{II}(MeCN)]$^{2+}$** species.

Comparison with analogous complexes of L$_5$^{2}-type ligands bearing 2 tertiary amines and 3 pyridines indicates a decrease of *ca.* 0.3 V for $E_{1/2}$, due to the more donating ability of amines which destabilizes the Fe^{II} state.[28]

The addition of HClO$_4$ to the complex in CD$_3$CN was followed by NMR (Fig. S8†). In the presence of 1 equiv. of HClO$_4$,

Fe remains coordinated to the cyclen core but the pyridine is protonated, as can be seen by comparison with the spectrum of the protonated ligand. This is confirmed by UV-vis spectroscopy, with the loss of $Fe^{II} \rightarrow$ py MLCT (Fig. S9†), and by cyclic voltammetry, with a shift of $E_{1/2}$ from 0.71 V *vs.* SCE to 1 V (Fig. S10†). Additionally, CV experiments show that the Fe (cyclen) moiety is very resistant to acid as it persists with up to 20 equiv. of $HClO_4$.

Reactivity

The catalytic activity of **[(cyclenCB–CH_2py)Fe^{II}(OTf)](OTf)** in aliphatic and aromatic hydroxylation as well as epoxidation was tested using cyclohexane, anisole and cyclooctene as substrates, and H_2O_2 and PhIO as oxidants, and compared with complexes with aminopyridine ligands (Table 1). With PhIO (entry 6), the complex is only active in epoxidation reactions, giving reasonable yields in line with those obtained with parent complexes with varying ligand denticities (entries 7–9). Reactivity with H_2O_2 is relatively poor on all substrates (entry 1), while parent complexes bearing two amines and pyridines (2 to 4 pyridyl groups) all display significant conversions towards aromatic hydroxylation,[32] and denticity-dependent conversions in epoxidation and aliphatic hydroxylation (entries 3–5). However, **[(cyclenCB–CH_2py)Fe^{II}(OTf)](OTf)** remains selective in the oxidation of anisole, as its counterparts. Indeed, aromatic hydroxylation is favored over demethylation and within aromatic hydroxylation products, the *ortho* position is favored, yielding 2-methoxyphenol in higher proportions than would be expected for a statistical site distribution. Epoxidation is also favored over dihydroxylation. Interestingly, when 1 equiv. of $HClO_4$ is added to the complex, reasonable conversions are restored in aromatic hydroxylation and epoxidation (entry 2).

Spectroscopic studies were performed to rationalize these observations.

Characterization of intermediates

Addition of O-atom donors. The addition of PhIO to a 1 mM solution of **[(cyclenCB–CH_2py)Fe^{II}(OTf)](OTf)** in MeCN was followed by stopped flow UV-vis spectroscopy at 20 °C (Fig. S11†). Slight growth of a signal is observed at 730 nm, which is assigned to the d–d transition of an Fe^{IV}=O species.[33] In line with this low conversion into the intermediate, the $Fe^{II} \rightarrow$ py MLCT transition at 412 nm is poorly affected, while it should vanish upon iron oxidation. Attempts to generate the intermediate with *m*CPBA were more efficient. The accumulation of the 730 nm chromophore is enhanced while the $Fe^{II} \rightarrow$ py MLCT vanishes, which can be partly due to better oxidation of iron but also to pyridyl protonation (and thus decoordination) by the *m*-Cl-benzoic acid side-product. Based on typical ε values of Fe^{IV}=O with polyazadentate ligands (270–400 M^{-1} cm^{-1}),[33–35] a conversion ranging between 22 and 32% with *m*CPBA and 15 and 22% with PhIO after 1000 s is obtained. As a matter of comparison, $[(TPEN)Fe^{IV}{=}O]^{2+}$ is accumulated in 88% yield after 26 s under the same conditions.[34] This difference is tentatively ascribed to the spin state of the starting Fe^{II} complex. Indeed, ^{1}H NMR of **[(cyclenCB–CH_2py)Fe^{II}(OTf)](OTf)** is in line with a diamagnetic species. The addition of a proton ($HClO_4$) induces decoordination and protonation of the pyridyl group but the spectrum still corresponds to the diamagnetic species. In contrast, $[(TPEN)Fe](PF_6)_2$ displays broadened and shifted resonances under the same conditions (room temperature), indicating a spin equilibrium displaced towards

Table 1 Oxidation of substrates by hydrogen peroxide and iodosylbenzene catalyzed by various complexes at room temperature.[a] % Yields are given with respect to the oxidant

Substrate				Anisole				Cyclooctene		Cyclohexane	
Products											
Entry	Oxidant	N_x[b]	Catalyst	*o*	*p*	*m*	PhOH	Epoxide	Diol	-ol	-one
1	H_2O_2	N_5	[(cyclenCB–CH_2py)Fe(OTf)](OTf)	17.6	4.5	0.7	5.9	2.2	0	2.4	0.7
2	H_2O_2	N_5	[(cyclenCB–CH_2py)Fe(OTf)](OTf) + $HClO_4$	32.8	5.6	0.56	6.7	9.4	0.2	3.7	0.4
3	H_2O_2	N_5	$[(L_5^2)Fe(OTf)](OTf)$[32]	66	7.1	6.3	10.2	48.1	0.3	34.5	18.4
4	H_2O_2	N_6	$[(TPEN)Fe](PF_6)_2$[32]	36	4	1	6	17	—	7	7
5	H_2O_2	N_4	$[(L_4^2)Fe(OTf)_2]$[32]	62.0	—	—	8.0	135[c]	—	59.4	17.4
6	PhIO	N_5	[(cyclenCB–CH_2py)Fe(OTf)](OTf)	—	—	—	—	25.6	3	—	—
7	PhIO	N_5	$[(L_5^2)Fe(OTf)](OTf)$	—	—	—	—	20	3	—	—
8	PhIO	N_6	$[(TPEN)Fe](PF_6)_2$	—	—	—	—	21	—	—	—
9	PhIO	N_4	$[(L_4^2)Fe(OTf)_2]$	—	—	—	—	30.4	0.8	—	—
10	H_2O_2	—	No catalyst	—	—	—	—	1.4	0.3	—	—
11	PhIO	—	No catalyst	—	—	—	—	4.6	2.7	—	—
12	H_2O_2	—	$Fe^{II}OTf_2$	—	—	—	—	4.0	0.3	10.8	4.0
13	PhIO	—	$Fe^{II}OTf_2$	—	—	—	—	27.3	5.4	—	—

[a] Fe/H_2O_2/anisole: 1/20/3000, Fe/PhIO/cyclooctene: 1/2/3000. Phenol, *o*-MeO–phenol, *p*-MeO–phenol, and *m*-MeO–phenol are denoted PhOH, o, p, and m, respectively. Fe/H_2O_2/cyclooctene: 1/20/800, Fe/PhIO/cyclooctene: 1/2/800. Cyclooctene oxide and cyclooctane-1,2-diol are denoted epox and diol, respectively. Fe/H_2O_2/cyclohexane: 1/20/800, Fe/PhIO/cyclohexane: 1/2/800. Cyclohexanol and cyclohexanone are denoted-ol and -one, respectively. All assays were performed under aerobic conditions. [b] Ligand denticity: N_x. [c] The yield above 100% is assigned to the auto-oxidation reactions under aerobic conditions.

a paramagnetic form.[36] Consequently, in solution, **[(cyclenCB–CH_2py)Fe^{II}(OTf)](OTf)** is predominantly present as the low spin and thus inert $[(cyclenCB–CH_2py)Fe^{II}(MeCN)]^{2+}$ form, while $[(TPEN)Fe]^{2+}$ is much more labile. As O atom transfer requires the initial binding of PhIO or *m*CPBA to the metal, it will be limited by the degree of lability of the complex. While poorly accumulated, once formed, Fe^{IV}=O remains active in epoxidation reactions (Table 1).

Addition of H_2O_2. Addition of 20 equiv. of H_2O_2 to a 1 mM solution of **[(cyclenCB–CH_2py)Fe^{II}(OTf)](OTf)** in MeCN was followed by stopped flow UV-vis spectroscopy at 20 °C (Fig. 2, S12†). The Fe^{II} → py MLCT transition at 412 nm disappears, in line with the expected oxidation of Fe^{II} to Fe^{III}. Concomitantly, a band grows at 550 nm over 10 s which then slightly decays. This λ_{max} value is close to that of the Fe^{III}(OOH) species reported in the literature.[6,32] However, when a solution of **[(cyclenCB–CH_2py)Fe^{II}(OTf)](OTf)** in MeCN ([Fe] = 1 mM, 0.1 M NBu_4PF_6, 293 K, Fig. S13†) was oxidized by electrolysis, presumably to a $[(cyclenCB–CH_2py)Fe^{III}(OH)]^{2+}$ species, a similar UV-vis absorption at 550 nm was observed.

EPR analysis of a sample collected at the maximum accumulation of the 550 nm chromophore shows a single low spin Fe^{III} species with parameters g = 2.414, 2.240, and 1.888 (Fig. 3a red, S14 and S15†). This set of values does not correspond with those of the parent $(N_5)Fe^{III}$(OOH) species (typically, g = 2.21–2.18, 2.12, 1.97 in the case of $[(L_5^2)Fe^{III}(OOH)]^{2+}$)[37] and more consistent with $[(N_5)Fe^{III}(OH)]^{2+}$.[38] Formation of a Fe^{III}(OH) species was corroborated by the EPR signal obtained upon addition of 2 equiv. of H_2O_2 to **[(cyclenCB–CH_2py)Fe^{II}(OTf)](OTf)** which yielded the same results as with 20 equiv. (Fig. S14†).

As a definitive EPR reference fingerprint, we used single crystals of **[(cyclenCB–CH_2py)Fe^{III}(OMe)](OTf)$_2$** that we obtained from an aerated solution of the Fe^{II} complex in MeOH (see Fig. 1 and the ESI†).

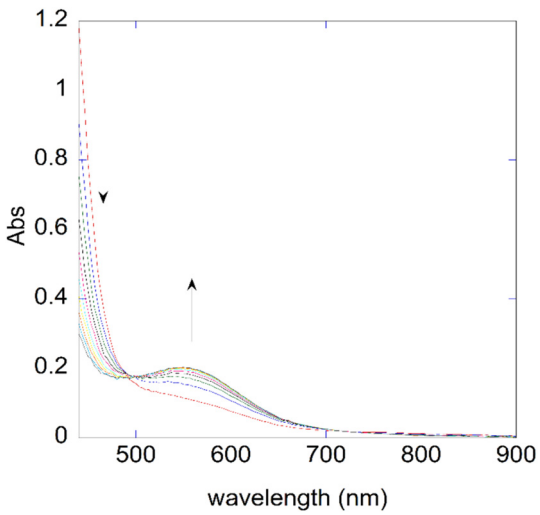

Fig. 2 Evolution of the UV-vis spectrum of **[(cyclenCB–CH_2py)Fe^{II}(OTf)](OTf)** (C = 1 mM) in MeCN (293 K), upon addition of 20 equiv. of H_2O_2: growth at 550 nm.

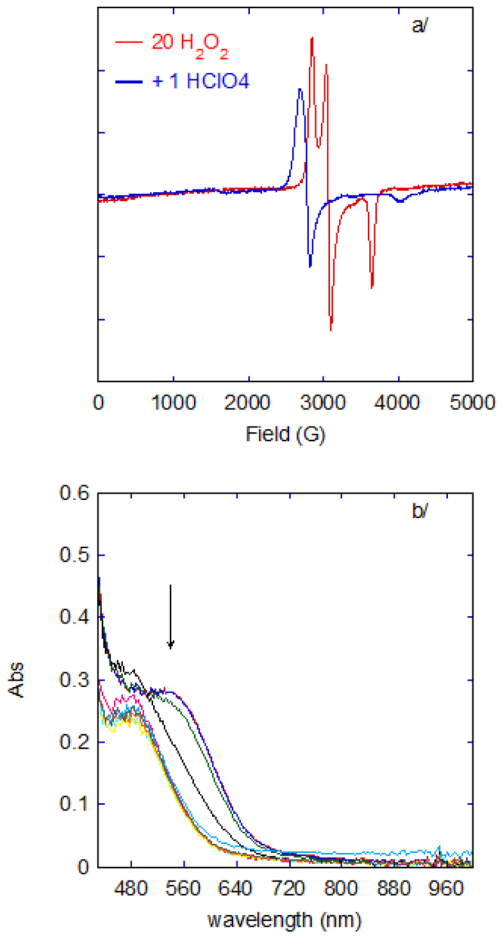

Fig. 3 Evolution of the X-band EPR spectra (90 K), (a/) and UV-vis spectrum (293 K, (b/) of the **[(cyclenCB–CH_2py)Fe^{II}(OTf)](OTf)**/H_2O_2 1 : 20 mixture solution (MeCN, [Fe] = 1 mM, aged 9 s at 293 K) upon addition of 1 equiv. of $HClO_4$. The EPR low spin signal represents 60% of the Fe content before the addition of $HClO_4$ and 46% after its addition.

In the literature, the structures of several $[(N_5)Fe^{III}(OMe)]^{2+}$ complexes have been reported with ligands bearing a mix of amines (N^{am}) and pyridines/benzimidazoles (N^{py}). In all cases, the Fe–O bond was around 1.78–1.88 Å. In one case, the small Fe–N bond lengths (1.96–2.01 Å) indicated a low spin species at 298 K, with a ($N_3^{am}N_2^{py}$)-type ligand based on triazacyclononane.[39] In another instance with a ($N_2^{am}N_3^{py}$)-type ligand, the complex was shown to display spin transition with temperature.[40,41] In all other cases ($N_2^{am}N_3^{py}$,[42–45] $N_1^{am}N_{44}^{py}$,[46] $N_0^{am}N_5^{py}$ type ligands[47]), at temperatures above 200 K, with Fe–N bond lengths between 2.1 and 2.3 Å, the complexes were more in line with high spin states. To the best of our knowledge, **[(cyclenCB–CH_2py)Fe^{III}(OMe)]$^{2+}$** is the first Fe^{III}–OMe complex bearing a $N_4^{am}N_1^{py}$ type ligand reported. With bond lengths of 1.84 Å for Fe–O and in the range 1.95–2.05 Å for Fe–N, the complex is in a low spin state. This is in agreement with the tendency of the above complexes, the low spin state becomes favoured with an increasing number of amine groups.

The EPR spectra showed a single species at g = 2.35, 2.18, and 1.92 in MeOH, and g = 2.38, 2.21, and 1.91 in MeCN

(Fig. S16†). These spectra are ascribed to **$[(N_5)Fe^{III}(OMe)]^{2+}$** in both cases, with the slight shift of the parameters being due to the protic nature of MeOH which can be hydrogen-bonded to the bound methoxo group.[48] The UV-vis signatures in MeCN and MeOH also display absorption at around 560 nm (Fig. S16†).

Thus, reaction of **$[(cyclenCB–CH_2py)Fe^{II}(OTf)](OTf)$** with 20 equiv. of H_2O_2 in MeCN does not lead to the accumulation of an $Fe^{III}(OOH)$ intermediate. For parent N_5 and N_6 types of complexes, MeOH has to be used as a solvent instead of MeCN to detect this species.[32,38]

When we changed the solvent to MeOH and added 20 equiv. of H_2O_2 to **$[(cyclenCB–CH_2py)Fe^{II}(OTf)](OTf)$**, we observed only EPR signals at g = 2.35, 2.18, and 1.92 ($(N_5)Fe^{III}(OMe)$) and g = 2.40, 2.21, and 1.91 ($(N_5)Fe^{III}(OH)$) (Fig. S17 and S18†).[6,48] Again, no $Fe^{III}(OOH)$ can be detected. However, when 100 equiv. of H_2O_2 were added to **$[(cyclenCB–CH_2py)Fe^{II}(OTf)](OTf)$** in MeOH, a small signal at g = 2.19, 2.15, and 1.955 can be seen (Fig. S17 and S19†), ascribed to an $(N_5)Fe^{III}(OOH)^{2+}$ species.[38] This is consistent with the disappearance of the g = 2.40, 2.21, and 1.91 resonances since $(N_5)Fe^{III}(OOH)^{2+}$ forms from a $(N_5)Fe^{III}(OH)^{2+}$ species (see the Discussion section). These observations indicate that $(N_5)Fe^{III}(OOH)$ forms but does not accumulate to a large extent.

This peculiar behaviour is likely related to the inertness of the complex. Unlike parent aminopyridine complexes, which are known to display spin equilibrium at room temperature in the Fe^{II} state,[36] the ligand field induced by cyclen strongly favors an Fe^{II} low spin state. This difference is likely transferred to the Fe^{III} state, making the Fe^{III} complex much more inert and reluctant to HO^-/HOO^- ligand exchange, and in turn, explains the low accumulation of the $Fe^{III}(OOH)$ intermediate and thus the low conversions in oxidation reactivity.

As the addition of $HClO_4$ induces a significant enhancement of reactivity, we followed the spectroscopic changes induced by the acid.

Addition of H_2O_2 in the presence of $HClO_4$. When one equiv. of $HClO_4$ is added to the solution at the apex of the accumulation of the 550 nm chromophore, the EPR signature changes immediately to give a new low spin Fe^{III} species with parameters g = 2.580, 2.475, and 1.710 (Fig. 3a (blue) and S20†).

The reaction can also be followed by stopped flow UV-vis spectroscopy (Fig. 3b). The **$[(cyclenCB–CH_2py)Fe^{II}(OTf)](OTf)$**/$H_2O_2$ 1 : 20 mixture solution was aged for 9 s at 293 K before adding 1 equiv. of $HClO_4$. In the first very fast step (0.02 s), the 550 nm chromophore vanishes to yield a new one at 480 nm. The latter then slowly decays to yield another chromophore at 450 nm (Fig. S21†).

In order to check if this new intermediate species is H_2O_2-related, we carried out the titration of **$[(cyclenCB–CH_2py)Fe^{III}(OMe)](OTf)_2$** by $HClO_4$ in MeCN by EPR (Fig. S22†).

The initial signal of **$[(cyclenCB–CH_2py)Fe^{III}(OMe)]^{2+}$** ($g$ = 2.38, 2.21, and 1.91) is gradually displaced towards a new one at g = 2.565, 2.465, and 1.725.

This signal (g = 2.565, 2.465, and 1.725) can be ascribed to two possible species with the following coordination spheres: a $[(N_5)Fe^{III}(MeCN)]^{3+}$, resulting from the protonation of the bound anion and its substitution by MeCN (eqn (1)):

$$\left[(\text{cyclenCB-CH}_2\text{py})\text{Fe}^{III}(\text{OMe})\right]^{2+} + \text{H}^+ + \text{MeCN} \leftrightarrows \left[(\text{cyclenCB-CH}_2\text{py})\text{Fe}^{III}(\text{MeCN})\right]^{3+} + \text{MeOH}; \quad (1)$$

or $[(N_4)Fe^{III}(OMe)(MeCN)]$ resulting from the protonation of the pyridine, its decoordination (the macrocyclic ligand becomes tetradentate) and the binding of an extra MeCN molecule (eqn (2)):

$$\left[(\text{cyclenCB-CH}_2\text{py})\text{Fe}^{III}(\text{OMe})\right]^{2+} + \text{H}^+ + \text{MeCN} \leftrightarrows \left[(\text{cyclenCB-CH}_2\text{pyH}^+)\text{Fe}^{III}(\text{OMe})(\text{MeCN})\right]^{3+}. \quad (2)$$

Given the strong Lewis acidity of Fe^{III}, it is very unlikely that **$[(cyclenCB–CH_2py)Fe^{III}(MeCN)]^{3+}$** would remain stable in solution (*e.g.* eqn (1) is highly unfavorable). The (g = 2.565, 2.465, and 1.725) signal can thus be ascribed to **$[(cyclenCB–CH_2pyH^+)Fe^{III}(OMe)(MeCN)]^{3+}$**.

When H_2O_2 was added to this solution (Fig. S23†), the residual signal of **$[(cyclenCB–CH_2py)Fe^{III}(OMe)]^{2+}$** disappeared, which suggests the displacement of the equilibrium towards a new species. However, only a slight change in the g values of the other species is detected: g = 2.58, 2.47, and 1.71 (Fig. S24†). The latter can be tentatively assigned to **$[(cyclenCB–CH_2pyH^+)Fe^{III}(OOH)(MeCN)]^{3+}$** (*i.e.* a $(pyH^+–N_4)Fe^{III}(OOH)(MeCN)$ species) which would have almost the same EPR signature as its methoxo counterpart (Scheme S1†).

To confirm this hypothesis, we carried out the experiment in MeOH where upon addition of $HClO_4$ to **$[(cyclenCB–CH_2py)Fe^{III}(OMe)]^{2+}$**, no changes were observed (Fig. S25a†) except for a slight drop in intensity, suggesting a dimerization process. This can be rationalized by the protonation of the pyridine leading to a $[(N_4)Fe^{III}(MeOH)(MeO)]^{2+}$ coordination sphere. Fe^{III}, being highly Lewis acidic, can be stabilized by sharing two bridging anions within a dimer. Upon addition of H_2O_2 to the previous solution, the intensity of the **$[(cyclenCB–CH_2py)Fe^{III}(OMe)]^{2+}$** signal decreases, and a new set of signals appeared at around g = 2.55 (Fig. S25b†), but no trace of the $(N_5)Fe^{III}(OOH)$ signal is detected, unlike what was observed in the absence of acid (see above). The addition of a second equivalent of the acid does not change the spectrum (Fig. S25c†), but the addition of extra H_2O_2 induced an increase of the signal intensity at g = 2.55 (Fig. S25d†). The experiments in MeOH (in the presence or absence of an acid) thus indicate that (i) in the absence of an acid, the addition of H_2O_2 to **$[(cyclenCB–CH_2py)Fe^{III}(OMe)]^{2+}$** generates $(N_5)Fe^{III}OOH$ in very limited quantities, in line with an intermediate that is difficult to accumulate (Scheme 1); (ii) addition of acid to **$[(cyclenCB–CH_2py)Fe^{III}(OMe)]^{2+}$** induces a drop in intensity, indicating that the expected mononuclear $[(pyH^+)\text{-}(N_4)Fe^{III}(MeOH)(OMe)]^{3+}$ species is not stable and dimerizes under these conditions, presumably forming a $(N_4)Fe^{III}(OMe)_2Fe^{III}(N_4)$ type dimer[49] or a $(N_5)Fe^{III}(O)Fe^{III}(N_5)$ one (Scheme 1); (iii) addition of H_2O_2 to this solution yields a new species with g_{max} = 2.55, which can thus likely be ascribed to the formation of a (N_4)

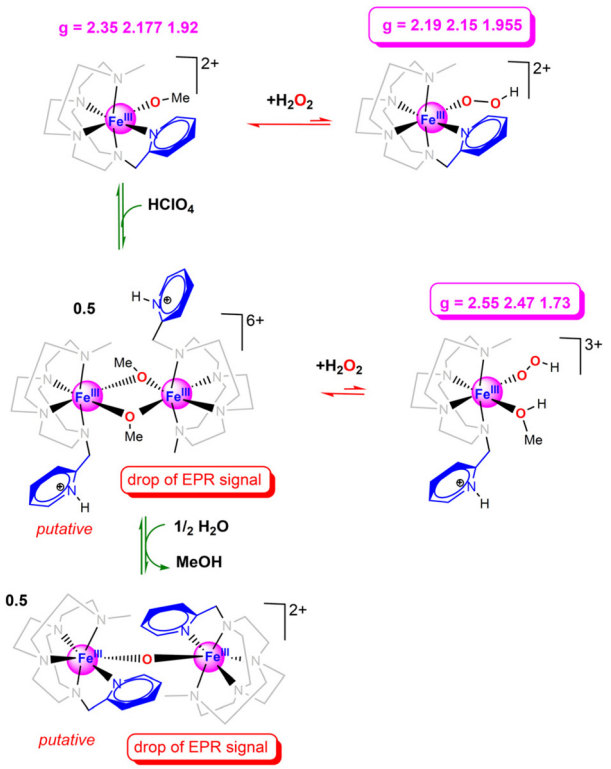

Scheme 1 Proposed species detected by EPR upon addition of $HClO_4$ and H_2O_2 to a **[(cyclenCB–CH_2py)Fe^{III}(OMe)]$^{2+}$** solution in MeOH.

Fe^{III}(OOH)(MeOH) species. Simulation of EPR for this species gives parameters g = 2.55, 2.47, and 1.73 (Fig. S26†). These conclusions are summarized in Scheme 1.

By analogy, in MeCN, a (pyH^+–N_4)Fe^{III}(OOH)(MeCN) species, with a dangling pyridinium, is expected to form under acidic conditions and its EPR signature is likely very similar to that of its methoxo counterpart (pyH^+–N_4)Fe^{III}(OOH)(MeOH).

Discussion

Cross-bridged tetraazamacrocycles are known for their ability to yield very stable[50] and inert[30,51,52] transition metal complexes[22,29–31,51,53–59] due to their extreme rigidity. Consequently, they have proven to be able to stabilize high oxidation states.[35,60–62] Such systems have been used in oxidation catalysis with iron[35,59,63,64] or manganese[61,65–68] complexes. In iron/H_2O_2 oxidizing systems, Hubin *et al.* showed results on the oxidation of thioanisole and the dehydrogenation of 1,4-cyclohexadiene,[59] Ruffo *et al.* reported the oxidation of alcohols,[64] and Que *et al.* studied epoxidation reactions.[63]

With the idea of increasing the "push" effect, we decided to increase the donating ability of our L_5^2 reference ligand in order to reexplore the oxidation ability of Hubin's ligand in comparative oxidation catalysis assays in aromatic, aliphatic hydroxylations and epoxidation reactions. Furthermore, as cross-bridged ligands yield highly acid-resistant complexes,[30,51,62] they also allowed us to explore a potential "pull" effect by working under acidic conditions.

Replacement of pyridines for secondary amines in ligand L_5^2 induces an increase of the donating ability of the ligand. This is reflected in lowering of the $Fe^{III/II}$ potential by 0.3 V and a significant push effect should be expected. But concomitantly, the increase of the number of σ-donors with no π-donor ability (amines) induces an increase of d orbital splitting. The low spin state of Fe^{II} is thus strongly favored as testified by the fully diamagnetic nature of the ^{1}H NMR spectrum of **[(cyclenCB–CH_2py)Fe^{II}(OTf)](OTf)** in MeCN, compared to its pyridine-containing L_5^2 or TPEN counterparts, which show spin equilibrium in solution at room temperature.[36]

[(cyclenCB–CH_2py)Fe^{II}(OTf)](OTf) shows relatively poor oxidation ability towards aliphatic or aromatic oxidation and alkene epoxidation with H_2O_2 compared to the L_5^2 or TPEN complexes. Upon addition of 1 equiv. of acid ($HClO_4$), the reactivity in aromatic oxidation is doubled, reaching those of the TPEN complex, while it is multiplied by four in the epoxidation of cyclooctene. Spectroscopic studies (UV-vis, EPR) were performed to identify the origin of this performance increase.

In MeCN, in the absence of acid, fast oxidation of Fe^{II} to Fe^{III} is observed upon H_2O_2 addition, but no accumulation of (N_5)Fe^{III}OOH can be detected. This is a classic behaviour observed with L_5^2 or TPEN complexes,[32] where (N_5)Fe^{III}OOH intermediates can be accumulated in large quantities when switching to a methanol solution.[38] However, in the case of **[(cyclenCB–CH_2py)Fe^{II}(OTf)](OTf)** in MeOH, only a very small amount of (N_5)Fe^{III}OOH can be detected by EPR, indicating that accumulation of the intermediate is very difficult. We propose that this difference arises from the high ligand field imposed by **cyclenCB–CH_2py**. The mechanism of (N_5)Fe^{III}(OOH) formation is a two-step process:

(i) oxidation of Fe^{II} (inner sphere)

$$(N_5)Fe^{II} + H_2O_2 \rightleftarrows (N_5)Fe^{III}(OH) + HO^{\bullet}$$

(ii) ligand substitution

$$(N_5)Fe^{III}(OH) + H_2O_2 \rightleftarrows (N_5)Fe^{III}(OOH) + H_2O$$

L_5^2 or TPEN Fe^{II} complexes, which show spin equilibrium at room temperature, are relatively labile given the amount of high spin species. In these cases, step (i) is very fast while step (ii) is slightly slower, but still much faster than the decay of the (N_5)Fe^{III}OOH intermediate, allowing its accumulation in solution.[37] With **[(cyclenCB–CH_2py)Fe^{II}(OTf)](OTf)**, the low spin state makes the complex much more inert, and as such, step (i) (inner sphere reaction) is slowed down due to slower ligand exchange. The low spin state is likely also favored at the Fe^{III} state, making step (ii) also slower to the point that if the rate of formation becomes close to the decay rate, the intermediate cannot be accumulated. This is in line with a previous example reported by our group in which the spin state of the complex, controlled by the binding mode of the ligand, had a drastic impact on the lability of the complex and thus on the reactivity in oxidation.[36]

In the presence of acid in MeCN, oxidation with H_2O_2 yields a new species observed at 480 nm with strongly split g factors (with g_{max} around 2.6). A similar species is observed upon addition of acid to **[(cyclenCB–CH$_2$py)Fe^{III}(OMe)]$^{2+}$**. This pattern is assigned to the coordination switch to a $[(N_4)Fe^{III}(MeCN)(X)]^{2+}$ species (X = OMe^-, OH^- or OOH^-) resulting from the protonation and decoordination of the pyridine group. In MeCN, the hydroxo and hydroperoxo species cannot be unambiguously distinguished by EPR. However in MeOH, the g_{max} = 2.6 species is only generated from **[((cyclenCB–CH$_2$py)Fe^{III}(OMe)]$^{2+}$** in the presence of both acid and H_2O_2 and its accumulation is enhanced with increasing amounts of H_2O_2, strongly suggesting that g_{max} = 2.6 is the signature of the $[(N_4)Fe^{III}(MeOH)(OOH)]^{2+}$ species. By analogy, the g = 2.58 species observed in MeCN in the presence of acid and H_2O_2 is assigned to $[(N_4)Fe^{III}(MeCN)(OOH)]^{2+}$. The enhancement of the $Fe^{III}OOH$ accumulation in acidic medium can be rationalized based on reactions (iii) and (iv)

(iii) pyridine protonation and decoordination

$$(N_5)Fe^{III}(OH) + H^+ + MeCN \rightleftarrows (pyH^+\text{–}N_4)Fe^{III}(MeCN)(OH)$$

(iv) ligand substitution

$$(pyH^+\text{-}N_4)Fe^{III}(MeCN)(OH) + H_2O_2 \leftrightarrows (pyH^+\text{-}N_4)Fe^{III}(MeCN)(OOH) + H_2O$$

Upon protonation and decoordination of pyridine in step (iii), the newly formed $(pyH^+\text{–}N_4)Fe^{III}(MeCN)(OH)$ is expected to display a lower ligand field (replacement of pyridine by MeCN). Consequently, the system becomes more labile and step (iv) becomes faster than step (ii) (Scheme 2). Furthermore, ligand exchange can now occur *via* MeCN exchange, the decoordination of which is easier than that of the anionic hydroxo. Finally, the dangling pyridinium could also act as a 2nd sphere acid moiety in step (iv), transiently protonating the bound hydroxo to aquo, further favoring ligand exchange.

The better accumulation of the $Fe^{III}(OOH)$ intermediate in the presence of an acid could explain the better performance during oxidation.

However, $Fe^{III}(OOH)$ is usually not proposed to be the reactive species, but a precursor to it. It can follow homolytic activation to form an {Fe^{IV}=O; OH$^\bullet$} pair, or a heterolytic cleavage to yield an Fe^{V}=O species (+OH^-). Complexes bearing pentadentate ligands are usually more prone to homolytic O–O bond cleavage in the absence of an acid,[5–9] while complexes based on tetradentate ligands were proposed to follow a heterolytic activation pathway when two exchangeable sites are present in *cis* positions.[11–15] This is due to the ability to stabilize the leaving hydroxo by coordination with Fe^{V}=O(OH) species. Finally, the addition of an acid to complexes of pentadentate ligands bearing a single exchangeable site can induce a shift in the activation pathway from homolytic to heterolytic, by protonation of the distal O atom in $Fe^{III}(OOH)$.[17–20]

In the **[(cyclenCB–CH$_2$py)Fe^{II}(OTf)](OTf)** case, the change in reactivity upon addition of an acid could also be tentatively assigned to such a switch in the activation pathway, as the system changes from a $(N_5)Fe^{III}(OOH)$ intermediate with a single exchangeable site to $(pyH^+\text{–}N_4)Fe^{III}(MeCN)(OOH)$ with two *cis* labile sites with an acidic moiety in the vicinity. This is also in line with the increase in the epoxidation yields. But in order to extract activation parameters to support these hypotheses, a significant accumulation of $Fe^{III}(OOH)$ is required, which is discarded here.

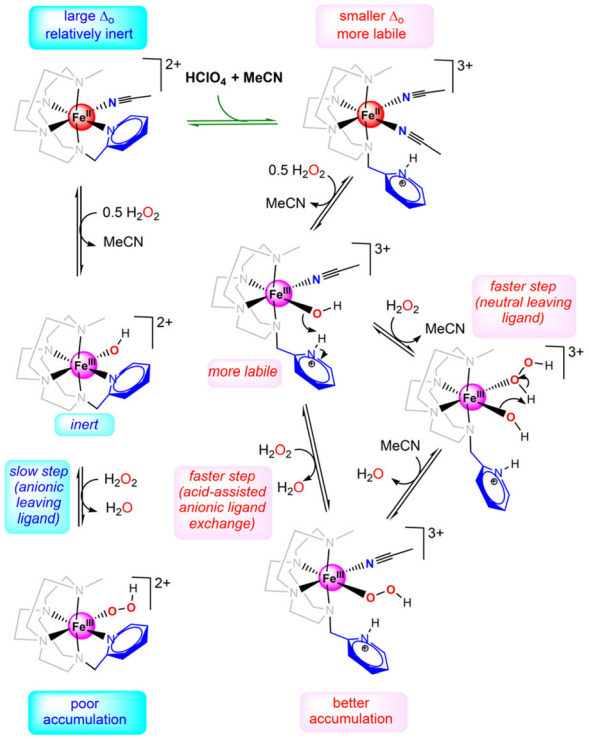

Scheme 2 Proposed species detected by EPR upon addition of $HClO_4$ and H_2O_2 to a **[(cyclenCB–CH$_2$py)Fe^{II}(MeCN)]$^{2+}$** solution in MeCN.

Conclusion

Herein, we report a new Fe^{II} complex derived from the ligand cyclenCB–CH_2py. Catalytic runs with H_2O_2 as an oxidant in reactions with anisole, cyclooctene and cyclohexane as substrates were carried out, showing activity towards aromatic oxidation and epoxidation. The backbone of the cross-bridged cyclen ligand allowed us to work under strongly acidic conditions without destruction of the complex and to explore the impact of the addition of an acid on the reactivity. One equivalent of $HClO_4$ significantly enhances the performance in anisole oxidation and cyclooctene epoxidation.

Spectroscopic studies were performed in order to rationalize these observations and showed that the intermediate switches from a $(N_5)Fe^{III}(OOH)$ intermediate to a $(pyH^+\text{–}N_4)Fe^{III}(MeCN)(OOH)$ one upon acid addition. The latter can be accumulated to a larger extent, which might explain the improved performance in oxidation. However, these changes could also be ascribed to a switch of mechanism in the acti-

vation of $Fe^{III}(OOH)$, from a homolytic O–O bond cleavage pathway to a heterolytic one. However, the poor accumulation of the intermediates prevented us from accessing activation parameters to support this hypothesis.

This lock is ascribed to the large ligand field induced by the tertiary amine ligands, which favor low spin states, making the system relatively inert. In order to circumvent this problem, we are currently working on ligand systems retaining this strong donating ability in order to generate a push effect favoring a heterolytic O–O activation process, while introducing a stronger π-donor character, in order to lower the ligand field and restore the lability that is necessary for catalysis.

Conflicts of interest

There are no conflicts to declare.

Acknowledgements

This work was supported by the LABEX CHARMMMAT (ANR-11-LABX-0039).

References

1 I. Bertini, A. Sigel and H. Sigel, *Handbook of metalloproteins*, Marcel Dekker, Inc, New York, 2001.
2 I. G. Denisov, T. M. Makris, S. G. Sligar and I. Schlichting, *Chem. Rev.*, 2005, **105**, 2253–2277.
3 B. Meunier, S. P. de Visser and S. Shaik, *Chem. Rev.*, 2004, **104**, 3947–3980.
4 P. R. Ortiz de Montellano, *Chem. Rev.*, 2010, **110**, 932–948.
5 A. Thibon, V. Jollet, C. Ribal, K. Sénéchal-David, L. Billon, A. B. Sorokin and F. Banse, *Chem. – Eur. J.*, 2012, **18**, 2715–2724.
6 O. V. Makhlynets and E. V. Rybak-Akimova, *Chem. – Eur. J.*, 2010, **16**, 13995–14006.
7 A. Company, L. Gomez, X. Fontrodona, X. Ribas and M. Costas, *Chem. – Eur. J.*, 2008, **14**, 5727–5731.
8 K. Chen, M. Costas, J. H. Kim, A. K. Tipton and L. Que, *J. Am. Chem. Soc.*, 2002, **124**, 3026–3035.
9 O. Cussó, X. Ribas and M. Costas, *Chem. Commun.*, 2015, **51**, 14285–14298.
10 A. S. Faponle, M. G. Quesne, C. V. Sastri, F. Banse and S. P. de Visser, *Chem. – Eur. J.*, 2015, **21**, 1221–1236.
11 I. Prat, A. Company, V. Postils, X. Ribas, L. Que, J. M. Luis and M. Costas, *Chem. – Eur. J.*, 2013, **19**, 6724–6738.
12 W. N. Oloo, R. Banerjee, J. D. Lipscomb and L. Que, *J. Am. Chem. Soc.*, 2017, **139**, 17313–17326.
13 I. Prat, J. Mathieson, M. Guell, X. Ribas, J. M. Luis, L. Cronin and M. Costas, *Nat. Chem.*, 2011, **3**, 788–793.
14 S. Xu, J. J. Veach, W. N. Oloo, K. C. Peters, J. Wang, R. H. Perry and L. Que, *Chem. Commun.*, 2018, **54**, 8701–8704.
15 M. Borrell, E. Andris, R. Navrátil, J. Roithová and M. Costas, *Nat. Commun.*, 2019, **10**, 901–909.
16 L. V. Liu, S. Hong, J. Cho, W. Nam and E. I. Solomon, *J. Am. Chem. Soc.*, 2013, **135**, 3286–3299.
17 F. F. Li, K. K. Meier, M. A. Cranswick, M. Chakrabarti, K. M. Van Heuvelen, E. Munck and L. Que, *J. Am. Chem. Soc.*, 2011, **133**, 7256–7259.
18 S. Kal, A. Draksharapu and L. Que, *J. Am. Chem. Soc.*, 2018, **140**, 5798–5804.
19 J. Serrano-Plana, F. Acuna-Pares, V. Dantignana, W. N. Oloo, E. Castillo, A. Draksharapu, C. J. Whiteoak, V. Martin-Diaconescu, M. G. Basallote, J. M. Luis, L. Que, M. Costas and A. Company, *Chem. – Eur. J.*, 2018, **24**, 5331–5340.
20 S. Xu, A. Draksharapu, W. Rasheed and L. Que, *J. Am. Chem. Soc.*, 2019, 16093–16107.
21 A. L. Robinson, J.-N. Rebilly, R. Guillot, C. Herrero, H. Maisonneuve and F. Banse, *Chem. – Eur. J.*, 2022, **28**, e202200217.
22 K. R. Wilson, D. J. Cannon-Smith, B. P. Burke, O. C. Birdsong, S. J. Archibald and T. J. Hubin, *Polyhedron*, 2016, **114**, 118–127.
23 G. R. Weisman, S. C. H. Ho and V. Johnson, *Tetrahedron Lett.*, 1980, **21**, 335–338.
24 G. R. Weisman, M. E. Rogers, E. H. Wong, J. P. Jasinski and E. S. Paight, *J. Am. Chem. Soc.*, 1990, **112**, 8604–8605.
25 G. R. Weisman, E. H. Wong, D. C. Hill, M. E. Rogers, D. P. Reed and J. C. Calabrese, *Chem. Commun.*, 1996, 947–948.
26 J. Rohovec, R. Gyepes, I. Cisarova, J. Rudovsky and I. Lukes, *Tetrahedron Lett.*, 2000, **41**, 1249–1253.
27 M. Le Baccon, F. Chuburu, L. Toupet, H. Handel, M. Soibinet, I. Dechamps-Olivier, J. P. Barbiere and M. Aplincourt, *New J. Chem.*, 2001, **25**, 1168–1174.
28 N. Ségaud, J.-N. Rebilly, K. Sénéchal-David, R. Guillot, L. Billon, J.-P. Baltaze, J. Farjon, O. Reinaud and F. Banse, *Inorg. Chem.*, 2013, **52**, 691–700.
29 T. J. Hubin, J. M. McCormick, S. R. Collinson, N. W. Alcock, H. J. Clase and D. H. Busch, *Inorg. Chim. Acta*, 2003, **346**, 76–86.
30 T. J. Hubin, J. M. McCormick, S. R. Collinson, M. Buchalova, C. M. Perkins, N. W. Alcock, P. K. Kahol, A. Raghunathan and D. H. Busch, *J. Am. Chem. Soc.*, 2000, **122**, 2512–2522.
31 T. J. Hubin, A. N. Walker, D. J. Davilla, T. N. Carder Freeman, B. M. Epley, T. R. Hasley, P. N. A. Amoyaw, S. Jain, S. J. Archibald, T. J. Prior, J. A. Krause, A. G. Oliver, B. L. Tekwani and M. O. F. Khan, *Polyhedron*, 2019, **163**, 42–53.
32 J.-N. Rebilly, W. Zhang, C. Herrero, H. Dridi, K. Sénéchal-David, R. Guillot and F. Banse, *Chem. – Eur. J.*, 2020, **26**, 659–668.
33 L. Que, *Acc. Chem. Res.*, 2007, **40**, 493–500.
34 M. Martinho, F. Banse, J. F. Bartoli, T. A. Mattioli, P. Battioni, O. Horner, S. Bourcier and J. J. Girerd, *Inorg. Chem.*, 2005, **44**, 9592–9596.

35 J. England, J. Prakash, M. A. Cranswick, D. Mandal, Y. S. Guo, E. Munck, S. Shaik and L. Que, *Inorg. Chem.*, 2015, **54**, 7828–7839.
36 K. Senechal-David, C. Buron, N. Segaud, J. N. Rebilly, A. Dos Santos, J. Farjon, R. Guillot, C. Herrero, T. Inceoglu and F. Banse, *Chem. – Eur. J.*, 2019, **25**, 12405–12411.
37 A. Bohn, C. Chinaux-Chaix, K. Cheaib, R. Guillot, C. Herrero, K. Sénéchal-David, J.-N. Rebilly and F. Banse, *Dalton Trans.*, 2019, **48**, 17045–17051.
38 M. Martinho, P. Dorlet, E. Riviere, A. Thibon, C. Ribal, F. Banse and J.-J. Girerd, *Chem. – Eur. J.*, 2008, **14**, 3182–3188.
39 N. W. Alcock, D. H. Busch and D. Zhang, *CCDC 219463: Experimental Crystal Structure Determination*, 2005.
40 N. Ortega-Villar, A. Y. Guerrero-Estrada, L. Piñeiro-López, M. C. Muñoz, M. Flores-Álamo, R. Moreno-Esparza, J. A. Real and V. M. Ugalde-Saldívar, *Inorg. Chem.*, 2015, **54**, 3413–3421.
41 N. A. Ortega-Villar, M. C. Muñoz and J. A. Real, *Eur. J. Inorg. Chem.*, 2010, **2010**, 5563–5567.
42 G. Wu, F. Mei, Q. Gao, F. Han, S. Lan, J. Zhang and D. Li, *Dalton Trans.*, 2011, **40**, 6433–6439.
43 P. Comba, H. Rudolf and H. Wadepohl, *Dalton Trans.*, 2015, **44**, 2724–2736.
44 F. Mei, C. Ou, G. Wu, L. Cao, F. Han, X. Meng, J. Li, D. Li and Z. Liao, *Dalton Trans.*, 2010, **39**, 4267–4269.
45 M. Lerch, A. J. Achazi, D. Mollenhauer, J. Becker and S. Schindler, *Eur. J. Inorg. Chem.*, 2021, **2021**, 4122–4132.
46 G. Roelfes, M. Lubben, K. Chen, R. Y. N. Ho, A. Meetsma, S. Genseberger, R. M. Hermant, R. Hage, S. K. Mandal, V. G. Young, Y. Zang, H. Kooijman, A. L. Spek, L. Que and B. L. Feringa, *Inorg. Chem.*, 1999, **38**, 1929–1936.
47 R. T. Jonas and T. D. P. Stack, *J. Am. Chem. Soc.*, 1997, **119**, 8566–8567.
48 J.-N. Rebilly, C. Herrero, K. Sénéchal-David, R. Guillot, T. Inceoglu, H. Maisonneuve and F. Banse, *Chem. Sci.*, 2021, **12**, 15691–15699.
49 F. Banse, V. Balland, C. Philouze, E. Riviere, L. Tchertanova and J. J. Girerd, *Inorg. Chim. Acta*, 2003, **353**, 223–230.
50 X. Sun, M. Wuest, G. R. Weisman, E. H. Wong, D. P. Reed, C. A. Boswell, R. Motekaitis, A. E. Martell, M. J. Welch and C. J. Anderson, *J. Med. Chem.*, 2002, **45**, 469–477.
51 T. J. Hubin, J. M. McCormick, S. R. Collinson, N. W. Alcock and D. H. Busch, *Chem. Commun.*, 1998, 1675–1676.
52 J. Pineau, L. M. P. Lima, M. M. Le Roy, S. Marionneau-Lambot, M. Cordier, P. Le Saëc, J. R. Zeevaart, C. H. S. Driver, A. Faivre-Chauvet, N. Le Bris and R. Tripier, *Chem. Commun.*, 2023, **59**, 888–891.
53 T. J. Hubin, J. M. McCormick, N. W. Alcock and D. H. Busch, *Inorg. Chem.*, 2001, **40**, 435–444.
54 T. J. Hubin, N. W. Alcock, M. D. Morton and D. H. Busch, *Inorg. Chim. Acta*, 2003, **348**, 33–40.
55 D. L. Maples, R. D. Maples, W. A. Hoffert, T. H. Parsell, A. van Asselt, J. D. Silversides, S. J. Archibald and T. J. Hubin, *Inorg. Chim. Acta*, 2009, **362**, 2084–2088.
56 T. J. Prior, D. L. Maples, R. D. Maples, W. A. Hoffert, T. H. Parsell, J. D. Silversides, S. J. Archibald and T. J. Hubin, *Acta Crystallogr., Sect. E: Struct. Rep. Online*, 2014, **70**, 148–152.
57 Z. Zhang, K. L. Coats, Z. Q. Chen, T. J. Hubin and G. C. Yin, *Inorg. Chem.*, 2014, **53**, 11937–11947.
58 D. G. Jones, K. R. Wilson, D. J. Cannon-Smith, A. D. Shircliff, Z. Zhang, Z. Q. Chen, T. J. Prior, G. C. Yin and T. J. Hubin, *Inorg. Chem.*, 2015, **54**, 2221–2234.
59 D. L. Matz, D. G. Jones, K. D. Roewe, M. J. Gorbet, Z. Zhang, Z. Q. Chen, T. J. Prior, S. J. Archibald, G. C. Yin and T. J. Hubin, *Dalton Trans.*, 2015, **44**, 12210–12224.
60 G. C. Yin, J. M. McCormick, M. Buchalova, A. M. Danby, K. Rodgers, V. W. Day, K. Smith, C. M. Perkins, D. Kitko, J. D. Carter, W. M. Scheper and D. H. Busch, *Inorg. Chem.*, 2006, **45**, 8052–8061.
61 G. C. Yin, A. M. Danby, D. Kitko, J. D. Carter, W. M. Scheper and D. H. Busch, *J. Am. Chem. Soc.*, 2007, **129**, 1512–1513.
62 K. J. Heroux, K. S. Woodin, D. J. Tranchemontagne, P. C. B. Widger, E. Southwick, E. H. Wong, G. R. Weisman, S. A. Tomellini, T. J. Wadas, C. J. Anderson, S. Kassel, J. A. Golen and A. L. Rheingold, *Dalton Trans.*, 2007, 2150–2162.
63 Y. Feng, J. England and L. Que, *ACS Catal.*, 2011, **1**, 1035–1042.
64 A. Annunziata, R. Esposito, G. Gatto, M. E. Cucciolito, A. Tuzi, A. Macchioni and F. Ruffo, *Eur. J. Inorg. Chem.*, 2018, 3304–3311.
65 G. C. Yin, M. Buchalova, A. M. Danby, C. M. Perkins, D. Kitko, J. D. Carter, W. M. Scheper and D. H. Busch, *J. Am. Chem. Soc.*, 2005, **127**, 17170–17171.
66 G. H. Yin, A. M. Danby, D. Kitko, J. D. Carter, W. M. Scheper and D. H. Busch, *Inorg. Chem.*, 2007, **46**, 2173–2180.
67 G. C. Yin, A. M. Danby, D. Kitko, J. D. Carter, W. M. Scheper and D. H. Busch, *J. Am. Chem. Soc.*, 2008, **130**, 16245–16253.
68 S. Shi, Y. J. Wang, A. H. Xu, H. J. Wang, D. J. Zhu, S. B. Roy, T. A. Jackson, D. H. Busch and G. C. Yin, *Angew. Chem., Int. Ed.*, 2011, **50**, 7321–7324.